

# Deflecting the Issue: The Origin of Nanoscale Material Build-up in Continuous Inkjet Printing

Maria Cristina Rodriguez-Rivero

*Institute for Manufacturing, Department of Engineering, University of Cambridge, UK*

*E-mail: mcr51@cam.ac.uk*

Julian M. Philpott, Alex B. Hann, and Josephine L. Harries

*Domino Printing UK, Cambridge, CB23 8TU, UK*

Ronan Daly

*Institute for Manufacturing, Department of Engineering, University of Cambridge, UK*

---

**Abstract.** *Continuous inkjet printing relies on steering charged droplets accurately to the surface by using electric fields. A vital component is the set of deflecting electrodes within the printhead, which create these fields. Unwanted deposition of ink on the electrodes, known as build-up, is a concern for operators because this modifies the applied electric field, affects long-term reliability, and requires manual intervention. However, this has not been widely reported or explored. Here, the authors report a laser-based high-speed visualization technique to observe build-up and show that it stems from small satellite droplets that break off from the main printed drops. They characterize the material build-up and reveal its nanoscale particulate nature. Combining the tracking with characterization allows quantifying the charge-to-mass ratio of these droplets. This study provides a route to understanding the build-up phenomenon, and it will enable optimization of printing conditions and printing reliability. © 2020 Society for Imaging Science and Technology.*

[DOI: 10.2352/J.ImagingSci.Technol.2020.64.5.050403]

---

## 1. INTRODUCTION

Industrial inkjet printing relies on the metered, uniform, and rapid generation of liquid ink drops directed to a surface where the formulated dye or pigment leaves a clear pattern. In continuous inkjet (CIJ) printing systems, a constant stream of drops is generated and, through capacitive charging and electrostatic repulsion, the drops are selectively deflected into specific patterns on the printed surface [1]. The working principle of CIJ relies on the phenomenon of Plateau-Rayleigh instability [2], where a continuous jet breaks up into droplets of equal size when subjected to controlled perturbation with the possibility of tuning the droplet size and inter-drop distance [3, 4]. The industrial applications of CIJ are often in marking or coding and are linked to regulatory requirements. This demands not only a high-level control of this phenomenon of instability but also high process reliability. It is critical to current production lines to deliver continuous printing with very low production

downtimes and minimal maintenance. Printers generate drops at frequencies of the order of 100 kHz ( $6 \times 10^{10}$  drops per week from a single jetting nozzle), and so error rates must be extremely low.

Printing defects from unsteady jetting or misalignment can occur in CIJ, with causes including full or partial nozzle blockage, insufficient or undetected droplet charging, condensation on detectors, and uneven jetting pressures. In this article, we focus on another key cause of defects, the phenomenon known as *build-up*, where materials are observed to deposit and grow in columns in or around the printhead, as shown in Figure 1. Over time, the growth of this material changes the applied electric field, and this leads to printing errors.

There are existing procedures and technologies that have been implemented to manage build-up. These include regular ‘wash-down’ procedures, which lead to printer downtime and exposure of the operator to volatile organic solvents. Alternatively, it has been noted that build-up can be reduced or avoided by locating the printing operation in areas that avoid sources of heat, stray electromagnetic fields, and electrostatic materials. Even more inconvenient measures include altering the printed code, print alignment, printer configuration, and even printer design. However, the phenomenon of material build-up is still poorly documented and described. In this article, we report a visualization technique to record the generation, deflection, and deposition of printed material leading to build-up. Build-up is identified for a range of operating conditions and two ink formulations, specifically a dye-based and a pigment-based ink. We study sub-micron-scale satellite drops and their deflected flight path using laser-based high-speed imaging techniques. We study the final chemical and physical nature of the build-up material and combine findings with droplet trajectory tracking information to estimate the charge-to-radius and charge-to-mass ratios for the deflected droplets. This provides the first step toward a better understanding of this industrial challenge and opens the door to mitigation strategies.

---

Received May 24, 2020; accepted for publication Aug. 13, 2020; published online Sep. 14, 2020. Associate Editor: Chunghui Kuo.

1062-3701/2020/64(5)/050403/10/\$25.00

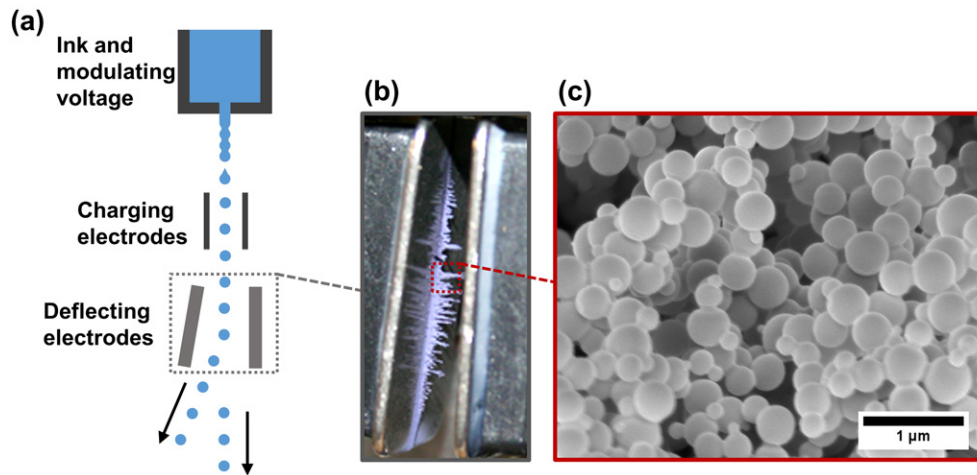


Figure 1. (a) Illustration of the working principle of CIJ, (b) image of material *build-up* on the CIJ deflecting electrodes, and (c) electron micrograph material deposited onto the deflecting electrode.

## 2. APPARATUS AND EXPERIMENTAL TECHNIQUES

### 2.1 Printing and High-speed Visualization

Figure 2 illustrates the experimental setup used in this study. Fig. 2(a) shows the visualization equipment layout, which is based on high-speed imaging. High-speed imaging techniques have been previously used to study in detail jet and drop formation [5] or airflows around inkjet printheads [6] due to the large amount of information that can be extracted from the printing process. The technique presented here was designed to perform time-resolved particle image velocimetry (t-PIV). A continuous diode laser (500 mW, 532 nm) is coupled to a 10 mm focal length planoconvex cylindrical lens (310 YD 25, Comar Optics) light source. The arrangement creates a laser sheet of approximately 1 mm in thickness. The cylindrical lens is placed 20 cm from the printhead. The sheet generated covers the desired field of view for the study (full length of the jet, 50 mm). The laser and lens are mounted at an angle to the horizontal to directly illuminate the full stream of drops in the printing path. A high-speed camera Phantom V710 is used with a 90 mm macro lens (Tamron) for imaging the full jet length, and a high magnification Precise Eye fixed lens system (Navitar) provides a field of view of 13.7 mm × 8.6 mm at full resolution (1280 × 800 pixels). All recordings (full length of the jet and closer visualization) are carried out between 7,000 and 20,000 fps with exposure times ranging from 49 μs to 120 μs. A smoke generator was used to seed and visualize airflows around the printhead for preliminary studies of the developed flows and their effect in terms of drag [6]. The printhead is installed at a horizontal position, and metallic surfaces are covered with black masking tape or are spray-painted black to avoid excessive light reflection and to allow visualization of the printing process, especially in the region of the deflecting plates.

A Domino A420i printing system was used, designed to issue ink under 3 bar of pressure. This system is equipped with two different printheads, the Classic and i-Tech heads,

which are both fitted with a 60 μm nozzle. A detailed schematic of the Classic printhead is provided in Fig. 2(b). Schematics of the different geometries of the deflecting plates for the two printhead models are presented in Fig. 2(d). In this work, the dye-based ink was printed with the Classic printhead and the pigment-based ink with the i-Tech printhead. Build-up has been previously reported in both printhead models and with both inks. As the research here deals with the origin of build-up with a focus on the origin of drops, a detailed comparison of printheads was considered out of scope. Therefore, the choices above were made to optimize experimental efficiency and avoid ink cross-contamination.

For the generation of droplets from the printer, a transducer receives a modulation signal for stimulating the ink acoustically and inducing regular jetting (Plateau-Rayleigh instability). The modulation signal is characterized by frequency and amplitude. Frequencies of 64 kHz and 84.5 kHz and various operating amplitudes (modulation voltage range) are used depending on the ink and the jetting pressure. The jetting pressure is directly related to the jetting velocity, which affects the development of the instability of the jet. Jetting pressure can be also adjusted (as voltage modulation) to tune the response to the stimulation of the jet. The charging signal is applied to the charging electrode to charge the droplets that need to be deflected. By “offset voltage,” we refer to a voltage measured between the ink ejecting gun of the printhead and the charging electrode when a charging voltage has not been deliberately applied to charge the drops. This potential difference is due to the behavior of the electronics of the printhead. The values of the offset voltage recorded in the reported experiments are insufficient to trigger the deviation of the main droplets from their path to the collecting gutter. The charging signal needs to have a suitable phase relationship with the drop formation and breakup, for which cycles of 10 V–12 V are applied to the charging electrode at intervals [7]. This process is known as phasing. Once again, the voltages applied for phasing are

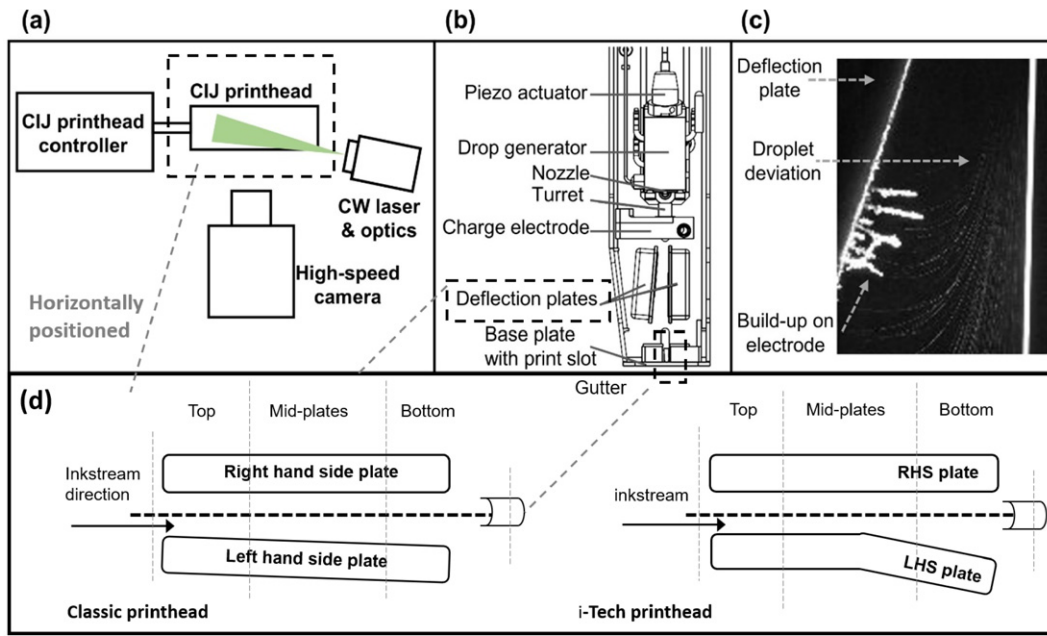


Figure 2. (a) Illustration of the visualization setup, (b) main components of a CIJ printhead, (c) visualized particles deviating from the main ink stream toward the LHS deflecting electrode, and (d) illustration of the horizontally oriented printhead (and deflecting plates) as used in the experimental setup.

insufficient to trigger the deviation of the main droplets from their path to the collecting gutter.

The printing process is characterized by the production of 60,000–100,000 drops per second at high velocity (approximately 20 m/s). The temporal and length scales of the process pose a challenge to traditional shadowgraphic optical imaging and require low exposure times and powerful lighting conditions to provide sufficient contrast between particles and the background. An example image is shown in Fig. 2(c), capturing the deflection plate, droplet deviation, and material build-up on the electrode. Three different inks are used in this study; all were developed for use with the Domino A420i CIJ printer. One dye-based black ink (BL1) is used as a control as there are no cases of deflector plate build-up reported for this ink. The second dye-based black ink (BL2) is known to exhibit moderate deflector plate build-up. The third pigment-based ink is a yellow ink (YL1) still under development that is found to exhibit considerable deflector plate build-up.

Build-up was previously observed with the chosen printing system under a specific range of printing conditions, which were targeted in this research. Modulation voltages were explored, ranging from 30 V to 150 V for BL1 and BL2 and from 30 V to 110 V for YL1. The jet was run at 3 bar for almost all experiments unless otherwise specified. The offset voltage was controlled between 0.48 and 0.82 V. Phasing was explored, with cycles of 10 V to 12 V applied to the charging electrode. All recorded experiments were carried out at a potential difference of 8.4 kV between the deflecting plates, which was the only deflecting voltage used when printing. Figure 3(a) shows an image stack covering the full length of the main ink stream while printing BL1 ink. Fig. 3(b–e) reveals droplets that emanate from various locations of the

main ink stream and arc toward the deflecting electrodes, all following paths of a similar profile.

## 2.2 Image Processing and Data Extraction

In most of the captured images, the light scattered by the small droplets of interest activates only one pixel, and this could vary in intensity from frame to frame. In addition, the level of contrast and lighting of every batch of experiments differs slightly due to the alignment of the light source, the visualization window chosen (top, middle, or bottom of the deflecting plates), and differences in the geometry of the printhead. Therefore, a slightly different image treatment is needed for each batch to distinguish the particle trajectories more sharply in contrast with the background. These modifications were helpful for ease of processing and the minimization of errors but did not change the observed trends. An example of a raw video and an optimized version are accessible through the link to supporting information at the end of this article to aid in the repeatability of the analysis. The image optimization was carried out using the Image Tools window of the acquisition software for the high-speed camera (PCC v.2.6.749.0 for 64-bit operating system) [8]. As an example, the videos of printing with YL1 ink, focused on the middle of the plates (see Fig. 3), were treated with an increased brightness of 1.11%, gain of 1.841, gamma of 2.222, saturation of 0, and manual white balance adjustment with red and blue values of 0.197 and 0.507, respectively. The videos for printing with BL2 ink, focused on the top of the plates (see Figure 4), were treated with a gain of 1.148, gamma of 2.222, saturation of 0, and manual white balance adjustment with red and blue values of 0.100 and 0.375, respectively. The build-up algorithm for color interpolation defined as medium in the software was used.

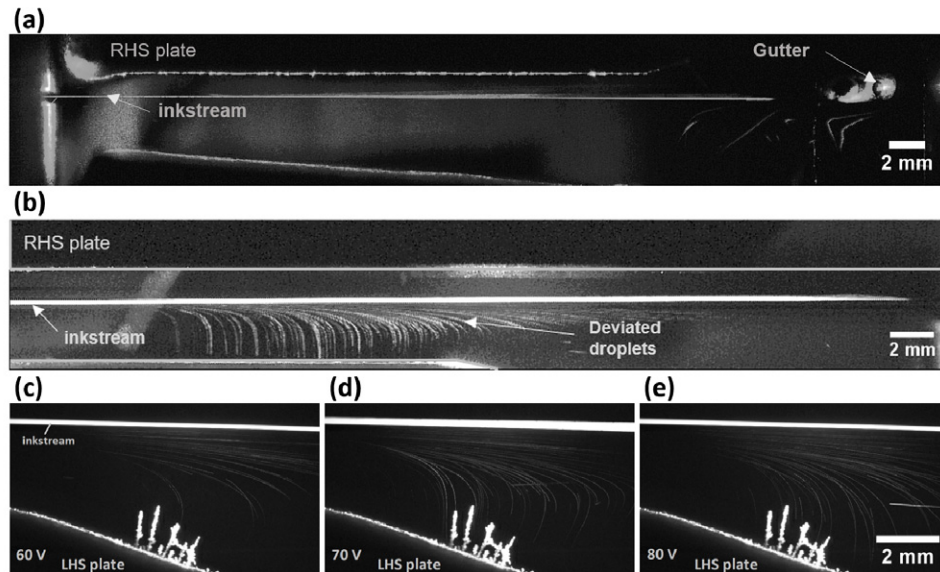


**Figure 3.** (a) Image stack showing printing of BL1 for the Classic printhead. The image covers a time frame of 64.9 ms with a modulation voltage of 85 V at 2.5 bar. (b) Image stack covering a time frame of 64.9 ms showing printing of the pigmented ink YL1 for the i-Tech printhead with a modulation voltage of 85 V at 2.5 bar. (c) Image stacks covering 21.58 ms of printing of ink YL1 for a modulation voltage 60 V, imaging the middle of the printhead deflecting places. (d) Repeated experiment at 70 V and (e) 80 V.

After image enhancement, ImageJ [9] was used to create image stacks from individual images. The resulting images show multiple different droplet trajectories and give good insights for identifying conditions under which droplets produce build-up. However, image stacks do not allow the extraction of quantitative information about individual particle trajectories, and so further information on the trajectories of the droplets was extracted using a particle tracking algorithm on Matlab. The main functions are “rgb2gray” to convert the images to grayscale, “imshow” to display a frame on the screen, and a loop with “impoint” and “wait” functions to allow selection of the particle to be tracked and to pass to the next frame for the selection of that same particle instants after the events seen on the previous frame. A selection (pixel) on the frame corresponds to the X and Y positions of the particle on that particular frame. These data for every frame are saved in a matrix. Consecutive frames in a batch of experiments are defined by a fixed time step, which is determined as the inverse of the video frame rate. Trajectories are obtained from the frame number and the particle position in that frame.

### 2.3 Analysis of Build-up Material

The chemical composition of deposited material is examined using a PerkinElmer system 2000 FTIR with an i-Series FTIR microscope and ATR objective. Spectra are reported, collected over  $4000\text{ cm}^{-1}$ – $700\text{ cm}^{-1}$  with 36 scans and spectra, and presented with their relative absorption normalized at the baseline. The size and morphology of the deposits are analyzed by scanning electron microscopy (SEM). The preparation for SEM analysis requires first that the inks are diluted in 2-propanol and then deposited on silicon surfaces to enable imaging of the dispersed components. A

thin conductive sputtered coating of gold/palladium is used to aid imaging. The ImageJ software is used to estimate particle size distribution. A minimum of 50 particles are randomly measured in each image. For the yellow pigment dispersion, 507 particles are measured across 6 images from two different samples; for the yellow ink build-up, 1190 particles are measured across 15 images from two different samples; and for the black ink build-up, 357 particles are measured across 5 images from two different samples. Each particle is measured for diameter in orthogonal directions to monitor for any non-unity aspect ratios. Statistical analysis is used to report quantiles, means, and standard deviations for populations, and a polydispersity index (PDI) is calculated for each sample set according to Eq. (1):

$$\text{PDI} = \frac{\langle d^2 \rangle}{\langle d \rangle^2}, \quad (1)$$

where  $d$  is the length of the longest aspect of each particle,  $\langle d^2 \rangle$  is the mean of the squared lengths, and  $\langle d \rangle^2$  is the square of the mean lengths.

## 3. RESULTS AND DISCUSSION

### 3.1 Visualization of Drop Deviation and Build-up

Build-up was previously observed with the chosen printing system under a specific range of printing conditions, which were targeted in this research. Modulation voltages were explored, ranging from 30 V to 150 V for BL1 and BL2 and from 30 V to 110 V for YL1. The jet was run at 3 bar for almost all experiments unless otherwise specified. The offset voltage was controlled between 0.48 V and 0.82 V. All recorded experiments were carried out under a potential difference of 8.4 kV between the deflecting plates, which was the only deflecting voltage used when printing. Fig. 3(a)

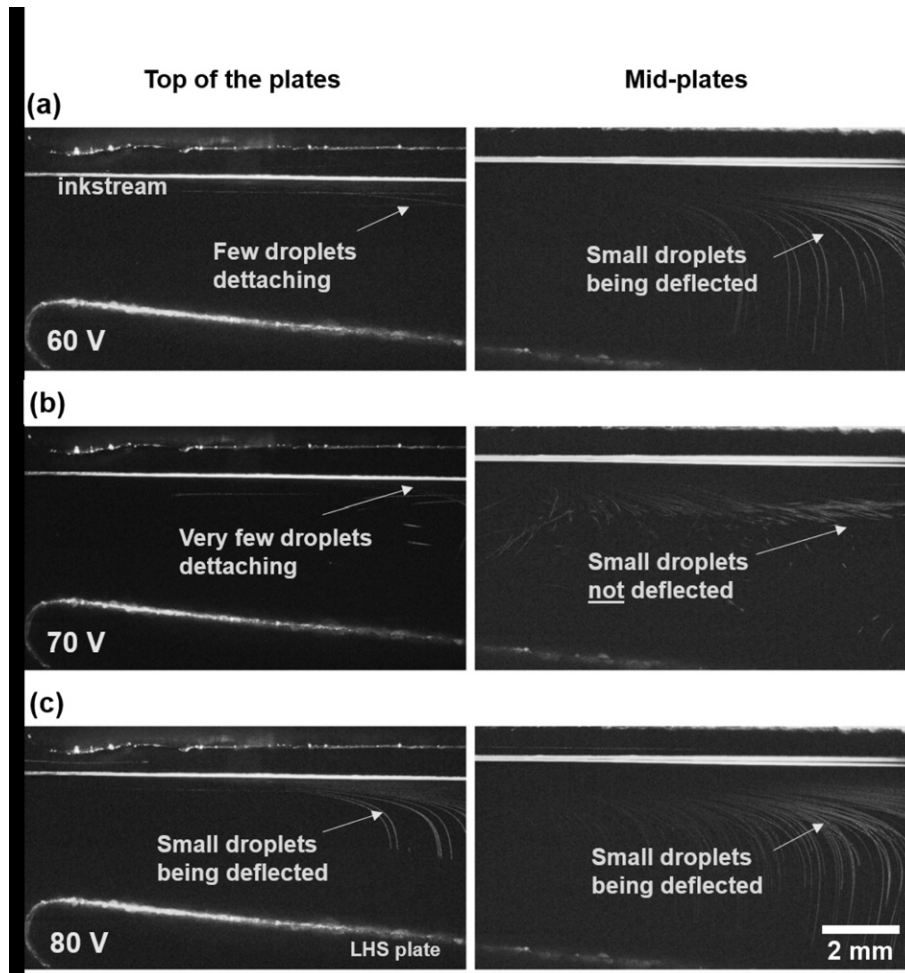


**Figure 4.** Image stacks covering 53.36 ms of printing of the black dye ink (BL2) for the Classic printhead for modulation voltages (a) 60 V, (b) 70 V, and (c) 80 V. Images show locations close to the top of the deflecting plates and around the middle of the deflecting plates of the printhead.

shows an image stack covering the full length of the main ink stream while printing BL1 ink for which no build-up has been reported. In comparison, Fig. 3(b) shows the main ink stream while printing YL1 ink. Fig. 3(b–e) reveals droplets that emanate from various locations of the main ink stream and arc toward the deflecting electrodes, all following paths of a similar profile.

In Fig. 3, we observe the printing behavior of YL1 ink for three different modulating voltages, 60 V, 70 V, and 80 V. These modulating voltages are in the middle of the tested range (30 V–110 V for this ink), where jet break-off has been reported and is expected to be optimal. In each case, imaging and visualization were carried out (Fig. 3c–e) at a higher magnification than that used for the image stack in Fig. 3(b), and images were again compiled into stacks. Fig. 3 shows the first directly observed evidence that build-up is due to small deflected droplets. Fig. 3(c–e) illustrates similar behavior and the number of particles responsible for the build-up. However, build-up generation is not independent of the modulation voltage, and we observe that more build-up is generated when the modulation voltages are at the lowest and highest values of the range of tested voltages (30 V

and 110 V), which are far from those reported as optimal values. These conditions are at the limit of the stable printing regime, and so it is highly likely that the origin of the small droplets imaged is in fact the satellite droplets generated during jet break-off. Figure 5 shows an image stack when pigmented ink (YL1) jets under the lowest value in its modulation voltage window (30 V). There are two scales of droplets observed with this visualization approach. The same level of small droplets is generated and deflected as seen in Fig. 3. We can conclude that these occur with and without phasing. However, during phasing, large droplets are generated and deflected toward the electrodes also. This results in a dramatic increase in material deposition, and so this study reveals that the phenomenon of material build-up is significantly exacerbated during phasing.

The dye-based ink (BL2) was also explored with modulation voltages being tested across the full printing window from 30 V to 150 V. Fig. 4 shows results from the middle of this range, 60 V–80 V. Again, the visualization technique allows the identification of conditions for which the systems generate fewer deflected droplets and therefore

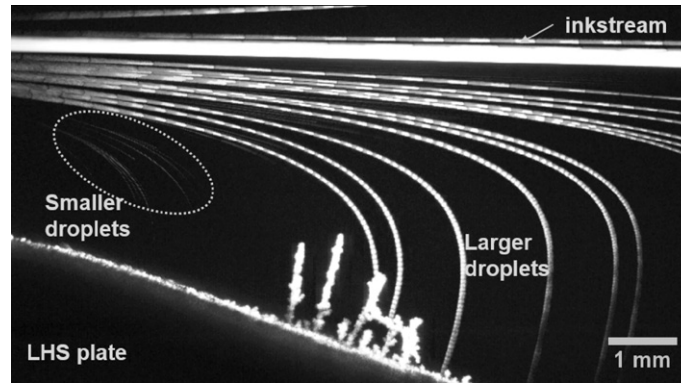


Figure 5. Stack of frames when pigmented ink jets at a modulating voltage of 30 V over 18.57 ms including phasing for the i-Tech printhead.

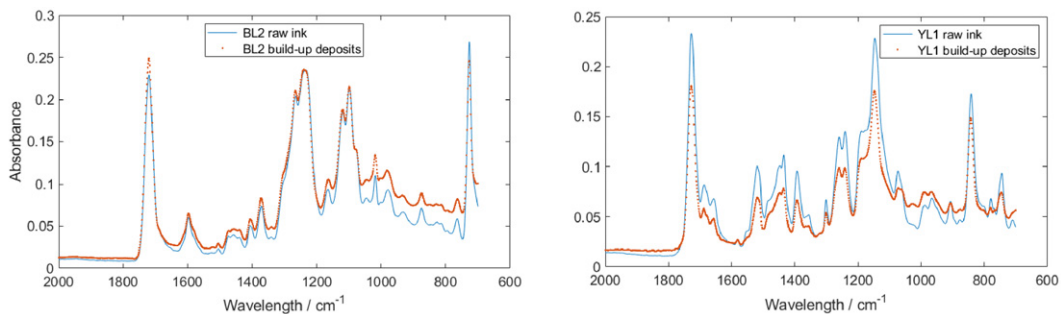


Figure 6. FTIR microscope spectra of bulk ink samples (solid lines) and build-up samples (dotted blue line).

less build-up such as for a modulation voltage of 70 V (Fig. 4(b)).

From visual inspection of the deposits, we observed that the deposition increases at locations higher on the plates as the offset voltage increases. This indicates a significant influence of the electric field in controlling the deviation of the droplets because a higher charge has been conferred. Furthermore, material build-up occurs exclusively along a single line on the plates in the plane of the electrostatic field and the main droplet stream. All of these observations indicate that the droplet matter is substantially charged, which confirms the occurrence of charging by inductance prior to or during break-off. To understand the process further, it was therefore critical to characterize the build-up material.

### 3.2 Material Characterization

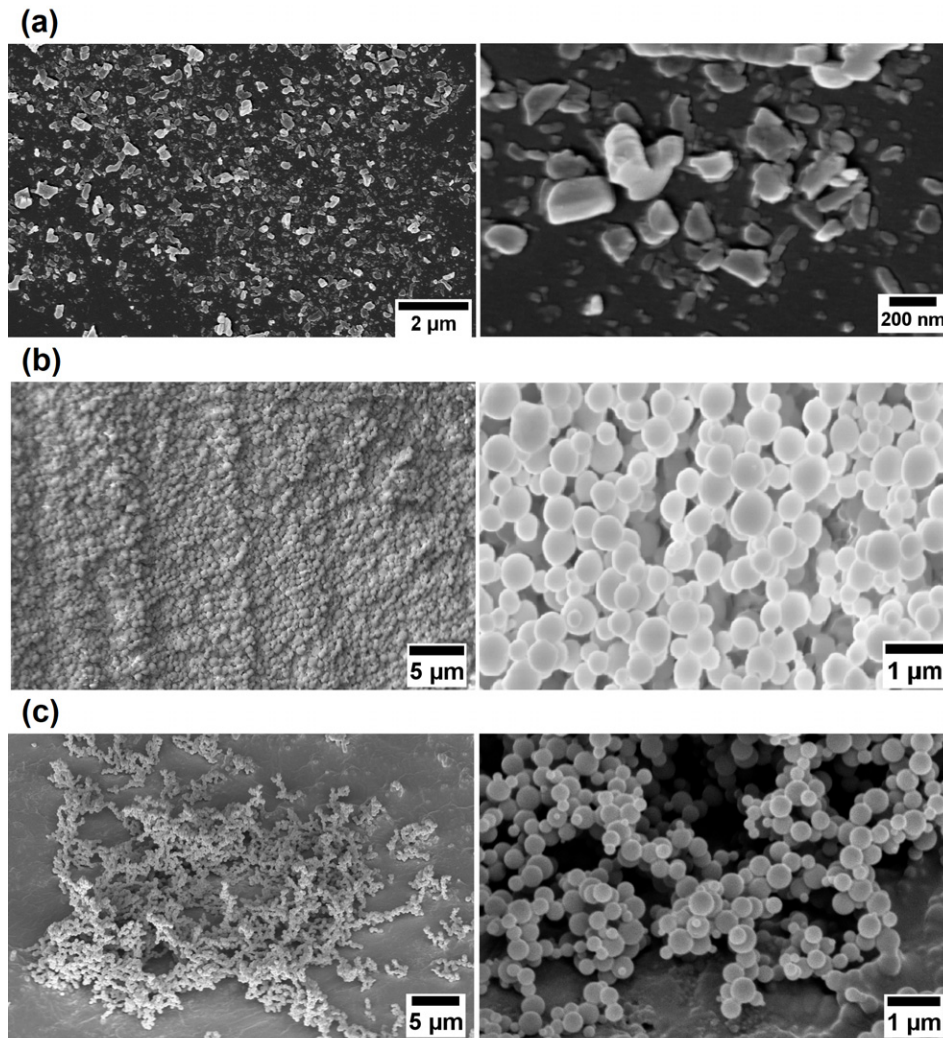
The material deposited on the deflector plates was collected for characterization by FTIR and SEM and compared against control samples of the bulk inks. The FTIR spectra (Figure 6), comparing both build-up deposits with their respective original bulk ink samples, demonstrate the presence of the same chemical groups in the same ratios. This indicates that the two are chemically near-identical, which first confirms that the build-up clearly originates only from the ink.

Figure 7(a) shows an SEM image of the pigments from the bulk YL1 ink. The pigment particles are milled crystalline organic materials, and hence they are non-uniform in shape with a high PDI. As observed in Fig. 7(a) and quantified in

Table I. Summary statistics for the particles analyzed from the SEM images.

	YL1 dispersion	YL1 build-up	BL2 build-up
Particle length (mean) / nm	126 ± 6	452 ± 8	324 ± 7
Particle length (median)/nm	95 ± 6	430 ± 8	348 ± 7
Polydispersity index	1.70	1.22	1.11
Aspect ratio (mean)	1.76 ± 0.08	1.13 ± 0.02	1.07 ± 0.02
Aspect ratio (median)	1.60 ± 0.08	1.09 ± 0.02	1.04 ± 0.02
Standard deviation	0.68	0.13	0.09

Table I, the yellow pigment dispersion has an average particle size of 126 nm with a PDI of 1.7. The particles have a mean aspect ratio of 1.76 (standard deviation of 0.68), indicating a high level of non-uniformity and a non-spherical nature. Interestingly, these measurements from the bulk ink are in stark contrast to those observed in the material build-up on the deflector plates for the yellow pigmented ink (YL1). As shown in Fig. 7(b) and Table I, the material build-up is composed of particles that are on average larger with a mean diameter of 452 nm and a smaller PDI of 1.22. The particles observed in the build-up are significantly more spherical than the pigment dispersion with a mean aspect ratio of 1.13. There are signs of some roughness and protuberances on the particles with an apparent radii of the order of 50 nm–100 nm, indicating that they contain the yellow pigment dispersion.



**Figure 7.** SEM images of (a) bulk yellow pigmented ink (YL1) and (b) build-up deposits from yellow pigmented ink (YL1) when they jet at a modulation voltage of 60 V with a voltage offset of  $-3$  V and (c) black dye ink (BL2) when it jets at a modulation voltage of 60 V with a voltage offset of  $-3$  V.

For the build-up of the black dye ink (BL2) observed on deflector plates, as shown in Fig. 7(c), we again observe clusters of sub-micron particles. In this case, the particles appear highly spherical. They have a mean diameter of 324 nm, a polydispersity index of 1.11, and a mean aspect ratio of 1.07. The spherical nature of these particles suggests a surface-tension-dominated process of formation, which matches our hypothesis of build-up composed of satellite droplets as observed earlier. The particles cluster in the build-up structure with the spherical particles being connected by necking behavior, suggesting that the whole solvent has not completely evaporated when the particles meet on the plate. The yellow ink build-up material shows greater particle lengths and polydispersity indices than those of the black ink build-up, indicating that larger satellites are formed during jetting. This is not necessarily linked to the formulations but rather to the satellites formed during this iteration of experiments.

The observations from the high-speed imaging system and the results from the characterization of the samples lead us to the confirmation that there must be an unexpected generation of satellites during jet break-off and a charging phenomenon of these satellites. Charging of liquid droplets has been extensively studied for the case where droplets are charged deliberately such as for the application studied here and other similar techniques such as electrospray [10, 11]. However, little or nothing has been explored for uncontrolled charging though some works point to phenomena during break-off as possible causes of systematic charging [12, 13]. We have not included the possible contribution of triboelectric effects from contact with air. However, given the systematic nature of the build-up, we think the major contribution arises from charge separation between droplets and hence electrostatic and Coulombic forces during the break-off and the disruption of the electrical double layer [14].

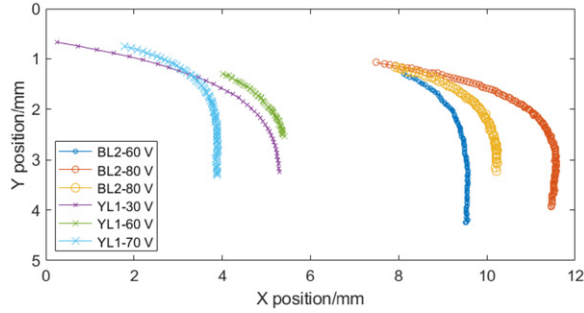


Figure 8. Trajectories for individual droplets under various printing conditions.

The aerosolized particles dry rapidly due to their large surface area-to-volume ratio. Some may exceed the Rayleigh charge stability limit during flight [15], inducing explosive dissociation of non-main ink stream droplets into charged particles [16]. By the time these particles land, they are almost free of the solvent and hence maintain their spherical form as they build up. The small amount of remaining solvent ensures some binding during the final drying stage, thereby allowing structures to form.

### 3.3 Estimation of Charge to Droplet Radius Ratio

The trajectories of particles were quantitatively analyzed from sequential images as explained in Section 2.2. Figure 8 shows representative trajectories for the droplets of both YL1 and BL2 inks. The droplets selected for analysis follow standard patterns under the corresponding printing conditions. The axis origin in Fig. 8 corresponds to the point where the main ink stream is seen to enter the imaging field of view. Therefore, the positions in the  $y$ -direction indicate the distance of the droplets from the main ink stream. It is not meaningful to compare the positions from the  $x$ -axis in Fig. 8 due to the different geometries of the printheads.

As discussed previously, the droplets are deflected in the direction of the  $y$ -axis due to their charge and their interaction with the electrostatic field. In the  $x$ -direction, the deceleration of the droplets is mostly due to drag forces though the angle of the left-hand-side (LHS) plates partly contributes to the deceleration along this axis owing to electrostatic force. The two main contributing forces on the droplets in the  $y$ -direction are the electrostatic force (Eq. (2)) and the drag force:

$$F_e = ma_e = qE. \quad (2)$$

Here,  $m$  and  $q$  are the mass and the charge of the droplet, respectively,  $a_e$  is the acceleration due to the electrostatic force, and  $E$  is the value of the electric field, which we assume to be a constant, and it results from the 8.4 kV potential difference over the 4.2 mm gap (the lowest plate separation).

Gravitational forces (weight and upthrust) are considered negligible since their effect is at least three orders of magnitude lower than the drag forces (true for droplets of size 20  $\mu\text{m}$  and less). Focusing on the balance of forces and motion in the  $y$ -direction, the expression of the drag force

on the droplets depends on the flow regime the droplets are subjected to, which is generally evaluated by the Reynolds number (Eq. (3)):

$$Re = \frac{\rho v D_d}{\mu}. \quad (3)$$

Here,  $\rho$  and  $\mu$  are the air density and the dynamic viscosity, respectively,  $v$  is the relative velocity of the droplet and the surrounding air, and  $D_d$  is the droplet diameter.

As mentioned in Section 2.1, preliminary observations of developed airflows showed that the  $x$ -component of the flow velocity decreases exponentially in the  $y$ -direction and becomes approximately 0.15 m/s at 1.7 mm from the ink stream in the positive  $y$ -direction. For reference, this is a change from about 20 m/s expected velocity at the center of the ink stream. Mostly, quiescent air is observed for higher values of  $y$ , depending on the region of the printhead. A more detailed study of the airflows will be addressed in future work to characterize the developed flows and fit the droplet trajectories. The preliminary observations of the flows within the printhead indicate laminar flow in between the plates with a decaying profile of the  $x$ -component velocity along the  $y$ -direction. The profile resembles a flow between parallel plates with a lower stationary plate and a moving upper plate with a negative nonzero pressure gradient ( $\partial p/\partial x$ ). This pressure gradient could be explained by the shape of the LHS plate acting as an expansion [17].

For the purpose of this study, we assume the  $y$ -component velocity of the air in between the jet and the LHS plate to be zero for the part of the trajectories that we have tracked. The values of the  $y$ -component velocity of the droplets can be extracted from the droplet trajectories as seen in Figure 9.

Fig. 9 shows that the particles attain terminal velocity along the  $y$ -axis (this is null acceleration) for the partial trajectory that could be visualized (see Figs. 5 and 7). The droplets could not be seen when they are very close to their detachment point from the main ink stream.

The values for the  $y$ -velocity of the sample droplets are presented in Table II. The Reynolds number for these velocities is lower than 1 for a theoretical droplet diameter of up to 30  $\mu\text{m}$ . We then apply the Stokes law of drag for creeping flow (Eq. (4)):

$$F_d = ma_d = -6\pi \mu r v_{rel}. \quad (4)$$

Here,  $m$  and  $r$  are the mass and the radius of the droplet, respectively,  $a_d$  is the acceleration due to the drag force,  $\mu$  is the air density, and  $v_{rel}$  is the relative velocity of the droplet and the surrounding air.

The balance of the two main contributing forces (Eq. (5)) allows us to estimate the charge-to-radius ratio, which is directly dependent on the terminal velocity measured as seen in Eq. (6):

$$qE = 6\pi \mu r v_T, \quad (5)$$

$$\frac{q}{r} = \frac{6\pi \mu v_T}{E}. \quad (6)$$

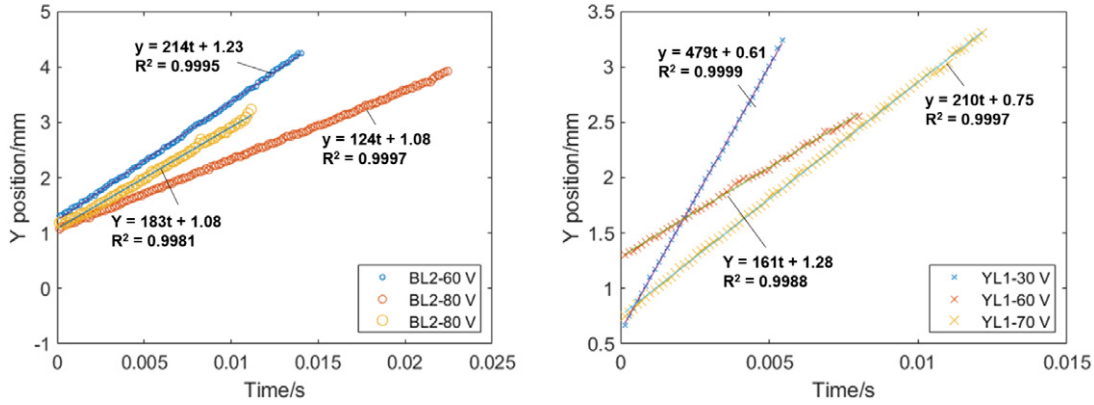


Figure 9. Particle position in the Y-axis as a function of time.

**Table II.** Values of parameters extracted and used for calculations.

Sample	Radius of initial drop (m)	Mass of initial drop (kg)	Rayleigh limit (C)	$v_T$ (m/s)	$q/r$ (C/m)	Charge per drop, $q_1$ (C)	$q/m$ (C/kg)	Charge per drop, $q_2$ (C)
YL1 60 V	$3.83 \times 10^{-7}$	$2.01 \times 10^{-16}$	$3.06 \times 10^{-15}$	0.156	$2.65 \times 10^{-11}$	$1.01 \times 10^{-17}$	$3.98 \times 10^{-3}$	$8.02 \times 10^{-19}$
YL1 70 V				0.204	$3.46 \times 10^{-11}$	$1.32 \times 10^{-17}$		
BL2 60 V	$2.54 \times 10^{-7}$	$5.87 \times 10^{-17}$	$1.66 \times 10^{-15}$	0.206	$3.49 \times 10^{-11}$	$8.87 \times 10^{-18}$		
BL2 80 V				0.120	$2.04 \times 10^{-11}$	$5.17 \times 10^{-18}$		
BL2 80 V				0.183	$3.10 \times 10^{-11}$	$7.88 \times 10^{-18}$		

The distance between the plates is not constant. However, for the purpose of estimation of the charge-to-radius ratio, we consider a constant value of the electrostatic field. The values of the estimated  $q/r$  ratios are presented in Table II, and they are approximately  $3 \times 10^{-11}$  C/m. For reference, the value of  $q/r$  for the sample YL1 of 30 V (droplets through phasing) is approximately twice. The later value could suggest that the application of a higher charging voltage (10 V–12 V compared to approximately 0.5 V in the other cases) could induce a larger charge on the droplets. However, we cannot conclude this firmly without a more precise measurement of the droplet radii. The volume of the droplets increases with  $r^3$ , which could mean that a larger charge is due to a larger volume of the droplet and not strictly due to a change in the applied voltage.

The initial size of the droplets can be estimated from the size of the dry deposited material observed through SEM (see Section 3.2). The solid content values of the bulk BL2 ink and bulk YL1 ink are 26 wt% and 20.6 wt% and their densities are  $857 \text{ kg/m}^3$  and  $858 \text{ kg/m}^3$ , respectively. We estimate the size of the initial drop before it detaches from the ink stream by considering the given density as average (values in Table II).

The sub-micron size of the initial droplets explains the difficulties in observing these satellites using standard shadowgraphic techniques. However, the charge-to-radius estimation shows a very low charge per drop ( $q_1$ ). This corresponds to an order of magnitude of 100 excess electrons. To check this finding, we also estimate the charge of the

droplets from their kinematics by considering the effect of the electric field and the trajectory. As per Eq. (7), the charge-to-mass ( $q/m$ ) ratio can be obtained:

$$h_y = \frac{1}{2} \frac{q}{m} E \left( \frac{h_x}{v_{0,x}} \right)^2. \quad (7)$$

Here,  $h_y$  and  $h_x$  are the distances the droplet travels under the influence of the electrostatic field along the indicated axes and  $v_{0,x}$  is the initial velocity of the particle in the  $x$ -direction (20 m/s in this case).

If 4.5 mm and 22 mm are the distances traveled in the  $y$ -direction (see Fig. 3) and the  $x$ -direction, respectively (as per the design of the printheads), the calculated value of the  $q/m$  ratio and the charge per drop ( $q_2$ ) for the estimated mass of the initial droplet are as given in Table II. This second approach to estimate the charge on the droplets only considers the contribution of the electric field to change the initial motion of the particles. It does not include the contribution of drag forces, and hence it presents a lower bound value for the charge of the droplets, which has a similar low order of magnitude.

Finally, for comparison and validation, the  $q/m$  ratio for the main ink stream droplets can be calculated by Eq. (8) when charged for deviation under standard printing conditions. This contains an additional term for the deviation of the droplet when it is not subjected to the electric field any

longer:

$$h_y = \frac{q}{m} E \frac{a}{v_{0,x}^2} \left( \frac{a}{2} + b \right). \quad (8)$$

Here,  $a$  is the total length of the deflecting plates and  $b$  is the distance traveled by the particles outside the field. An example of normal printing conditions is denoted by the following values:  $a = 32$  mm,  $b = 48$  mm,  $h_y = 12$  mm, and the mass of the drop  $m = 5.70 \times 10^{-10}$  kg. By applying these values,  $1.26 \times 10^{-3}$  C/kg is obtained as the  $q/m$  ratio and  $7.16 \times 10^{-13}$  C as the charge on the droplet. This corresponds to an order of magnitude of  $10^6$  excess electrons, which agrees with that defined by Kuhn and Myers [18] in an important early description of the technology. Further work to characterize the sub-micron drop volumes would enable much more accurate estimation of the charge per droplet of the satellites leading to the build-up phenomenon.

#### 4. CONCLUSIONS

This work shows that the phenomenon of particulate deposits observed on the deflecting plates of CIJ printheads, known as *build-up*, has its origin in the ink stream ejected from the nozzle and specifically the electrostatic field generated by the deflecting plates acting on sub-micron satellite ink droplets. The visualization technique developed for this work allows us to observe these clearly and also monitor their behavior with changes in modulation voltage and phasing. This visualization technique allows us to extract quantitative information from the trajectories of the deflected particles and obtain an estimation of the charge-to-radius ratio and the charge-to-mass ratio, while material characterization shows that the deposited droplets reach the deflection electrodes free of solvent in the form of sub-micron particles. It also shows a transition to low polydispersity index for some of the collected deposited particles. However, the calculations indicate a very low charge per drop, which could be due to an underestimated droplet size, based on SEM images.

In summary, we have reported a newly developed approach to monitor and characterize a common challenge for the digital printing technology, CIJ. We have overcome the complications encountered by conventional shadowgraphic imaging techniques to visualize the build-up process and have suggested an initial physical model. This work also has implications in the study of processes that show unintended or undesirable charging behavior in fluids such as DoD

printing, pipetting [19], splashing [20], and capillary phenomenon in microfluidics [21] and aerosols [13]. In addition, it encourages further studies on systematic charging of droplets not subjected to intended electrical fields.

#### SUPPLEMENTARY MATERIAL

Supplementary data that have been mentioned in the text are available online (<https://doi.org/10.17863/CAM.55964>).

#### ACKNOWLEDGMENT

The authors would like to acknowledge the analytical work of Sheila M. Stevens and The Welding Institute, Cambridge, UK, for their help with FTIR measurements and interpretation of spectra.

#### REFERENCES

- H. P. Le, "Progress and trends in ink-jet printing technology," *J. Imaging Sci. Technol.* **42**, 49 (1998).
- L. Rayleigh, "On the instability of jets," *Proc. Lond. Math. Soc.* **1**, 4 (1878).
- C. Weber, "Zum Zerfall eines Flüssigkeitsstrahles," *ZAMM-J. Appl. Math. Mech./Zeitschrift Für Angew. Math. Und Mech.* **11**, 136 (1931).
- D. B. Bogy, *Annu. Rev. Fluid Mech.* **11**, 207 (1979).
- I. M. Hutchings, G. D. Martin, and S. D. Hoath, "High speed imaging and analysis of jet and drop formation," *J. Imaging Sci. Technol.* **51**, 438-444 (2007).
- C. Rodriguez-Rivero, J. R. Castrejon-Pita, and I. M. Hutchings, "Aerodynamic effects in industrial inkjet printing," *J. Imaging Sci. Technol.* **59**, 40401 (2015).
- G. D. Martin, S. D. Hoath, and I. M. Hutchings, *J. Phys. Conf. Ser.* **105**, 12001 (2008).
- Vision Research Inc., <https://www.phantomhighspeed.com/> (n.d.).
- C. A. Schneider, W. S. Rasband, and K. W. Eliceiri, *Nat. Methods* **9**, 671 (2012).
- R. H. Magarvey and B. L. Blackford, *J. Geophys. Res.* **67**, 1421 (1962).
- Y. Huo, J. Wang, Z. Zuo, and Y. Fan, *Phys. Fluids* **27**, 114105 (2015).
- P. R. Jonas and B. J. Mason, *Trans. Faraday Soc.* **64**, 1971 (1968).
- L. W. Zilch, J. T. Maze, J. W. Smith, G. E. Ewing, and M. F. Jarrold, "J. Phys. Chem.," **A 112**, 13352 (2008).
- J. V. Iribarne and B. J. Mason, *Trans. Faraday Soc.* **63**, 2234 (1967).
- L. Rayleigh, "London, Edinburgh," *Dublin Philos. Mag. J. Sci.* **14**, 184 (1882).
- C. B. Richardson, A. L. Pigg, and R. L. Hightower, *Proc. R. Soc. Lond. A. Math. Phys. Sci.* **422**, 319 (1989).
- P. K. Kundu, I. M. Cohen, and D. R. B. T. Dowling, *Laminar Flow, Fluid Mechanics*, 5th ed. (Academic Press, 2012), pp. 309-359.
- L. Kuhn and R. A. Myers, *Sci. Am.* **240**, 162 (1979).
- D. Choi, H. Lee, D. J. Im, I. S. Kang, G. Lim, D. S. Kim, and K. H. Kang, *Sci. Rep.* **3**, 2037 (2013).
- N. Miljkovic, D. J. Preston, R. Enright, and E. N. Wang, *Nat. Commun.* **4**, 2517 (2013).
- F. Malloggi, D. van den Ende, and F. Mugele, *Langmuir* **24**, 11847 (2008).